Iron colloids dominate sedimentary supply to the ocean interior

William B. Homoky[a,b,1], Tim M. Conway[c], Seth G. John[d], Daniela König[e], FeiFei Deng[b], Alessandro Tagliabue[e], and Rachel A. Mills[f]

[a]School of Earth and Environment, University of Leeds, Leeds LS2 9JT, United Kingdom; [b]Department of Earth Sciences, University of Oxford, Oxford OX1 3AN, United Kingdom; [c]College of Marine Science, University of South Florida, Tampa, FL 33629; [d]Department of Earth Sciences, University of Southern California, Los Angeles, CA 90007; [e]School of Environmental Sciences, University of Liverpool, Liverpool L69 3GP, United Kingdom; and [f]School of Ocean and Earth Science, University of Southampton, Southampton SO17 1BJ, United Kingdom

Edited by Donald E. Canfield, University of Southern Denmark, Odense M., Denmark, and approved January 25, 2021 (received for review July 29, 2020)

Dissolution of marine sediment is a key source of dissolved iron (Fe) that regulates the ocean carbon cycle. Currently, our prevailing understanding, encapsulated in ocean models, focuses on low-oxygen reductive supply mechanisms and neglects the emerging evidence from iron isotopes in seawater and sediment porewaters for additional nonreductive dissolution processes. Here, we combine measurements of Fe colloids and dissolved δ^{56}Fe in shallow porewaters spanning the full depth of the South Atlantic Ocean to demonstrate that it is lithogenic colloid production that fuels sedimentary iron supply away from low-oxygen systems. Iron colloids are ubiquitous in these oxic ocean sediment porewaters and account for the lithogenic isotope signature of dissolved Fe (δ^{56}Fe = +0.07 ± 0.07‰) within and between ocean basins. Isotope model experiments demonstrate that only lithogenic weathering in both oxic and nitrogenous zones, rather than precipitation or ligand complexation of reduced Fe species, can account for the production of these porewater Fe colloids. The broader covariance between colloidal Fe and organic carbon (OC) abundance suggests that sorption of OC may control the nanoscale stability of Fe minerals by inhibiting the loss of Fe(oxyhydr)oxides to more crystalline minerals in the sediment. Oxic ocean sediments can therefore generate a large exchangeable reservoir of organo-mineral Fe colloids at the sediment water interface (a "rusty source") that dominates the benthic supply of dissolved Fe to the ocean interior, alongside reductive supply pathways from shallower continental margins.

ocean sediment | porewater | iron colloid | organo-mineral | iron isotopes

Sediments undergo early diagenetic transformations that are understood to provide an important source of dissolved iron (dFe) to the ocean that is used to fuel primary production and secondary food webs, fix nitrogen, and support the air–sea transfer of carbon dioxide (1, 2). Nevertheless, fundamental questions remain concerning the magnitude of dFe released from ocean sediments and the mechanisms through which this supply may be moderated. Such uncertainty is most acute in oxic and deep-water regions, which bear the fewest observations, but represent the largest area of the ocean sediment–water interface (3). Here, comparatively small sedimentary releases of dFe have the cumulative potential to enhance the dFe inventory of the deep ocean and—in so far as it connects with surface water—relieve iron deficiency for phytoplankton. Porewaters in these deep-water regions maintain a persistently oxic and/or nitrogenous state adjacent to bottom waters that is largely unexamined for its role in the marine iron cycle. These gaps in knowledge hinder our ability to make more accurate simulations of the carbon cycle in ocean biogeochemical models (4).

Two principle processes are thought to be driving Fe dissolution from sediments that underpin the magnitude and variability of dFe inputs to the ocean. The first is a reductive-dissolution (RD) process, which demonstrably occurs during early diagenetic oxidation of organic carbon (OC) and produces high abundances of reduced, soluble, and isotopically light Fe in ferruginous porewaters, generally beneath the Fe-oxidizing fronts of nitrous oxides and oxygen (5–7). The second is a nonreductive-dissolution (NRD) process to account for the comparatively unfractionated or heavy isotope compositions of dFe attributed to sedimentary inputs in some oxygenated regions of the open ocean (8) and in the oxic zones of marine sediment porewaters (9), but the mechanisms governing so-called NRD in oxic sediments are unclear.

RD of Fe is coupled to OC oxidation and is widely observed in shallow porewater in sediments with high-oxygen consumption rates, under productive shelf seas, near zones of upwelling, and overlain by oxygen-depleted seawater (10). Low seawater oxygen content serves to enhance the efflux of reduced and soluble Fe (sFe, filtered <0.02 μm) from ferruginous porewaters and enables sFe(II) to propagate further in the water column (11–14). Subsequently, without sufficient chelation by organic ligands sFe(II) will be lost to oxidative precipitation (7, 15, 16), scavenging (12), and sedimentation in deeper water (16, 17). Sedimentary RD provides a key component of the ocean's dFe inventory that is most pronounced in the upper ocean (1, 10, 11, 13). It is also the only mechanism by which most ocean biogeochemical models simulate the sedimentary release of dFe (4), since model parameterizations rely on empirical relationships between dFe fluxes, OC oxidation rates, bottom water oxygen contents, and/or water depth (1, 11, 18, 19).

Significance

Phytoplankton assimilate carbon dioxide, produce oxygen, and nourish food webs on a scale that impacts planetary processes but are limited by iron deficiency over much of the global surface ocean. Therefore, we must understand processes that regulate the ocean's iron inventory to accurately simulate and predict the ocean's response to change. This study reveals that the widespread production of nanosized iron colloids from the weathering of lithogenic material drives sedimentary iron supply throughout the deep ocean. The discovery accounts for the unexplained occurrence of colloids and patterns of iron isotope variation previously observed in other parts of the deep ocean and suggests how long-standing assumptions we have used to simulate iron supply in ocean models must be revised.

Author contributions: W.B.H. and R.A.M. designed research; W.B.H. performed research; W.B.H., T.M.C., S.G.J., D.K., F.D., and A.T. contributed analytic tools; W.B.H., T.M.C., S.G.J., D.K., F.D., and A.T. analyzed data; and W.B.H., T.M.C., S.G.J., D.K., F.D., A.T., and R.A.M. wrote the paper.

The authors declare no competing interest.

This article is a PNAS Direct Submission.

[1]To whom correspondence may be addressed. Email: w.homoky@leeds.ac.uk.

This article contains supporting information online at https://www.pnas.org/lookup/suppl/doi:10.1073/pnas.2016078118/-/DCSupplemental.

Published March 26, 2021.

NRD is a term previously used to describe a sedimentary source of isotopically heavy dFe to the water column (8) and has since been used to describe the presence of lithogenic isotope compositions observed in oxidizing zones from some deep ocean sediment porewaters (9). Similar observations have become commonplace in the ocean interior (20–23), such that nonreductive sedimentary processes appear to be important for the ocean's dFe inventory. However, the detection of lithogenic dFe isotope signatures in porewaters (6, 9), within western North Atlantic benthic nepheloid layers, and in the water column far from sediment sources have been difficult to explain (24). The role played by this additional source of dFe is not yet included in global ocean models.

Based on the very low solubility of silicate minerals and Fe(III) oxides in circumneutral pH and oxygenated seawater, NRD ought to be incapable of sustaining a benthic flux of dFe to the ocean without significant chelation by organic ligands (25). Because of a strong isotope fractionation effect, however, ligand complexation of Fe would produce a much heavier Fe isotope signal in the ocean (26), which is at odds with the isotopic evidence for NRD (20–23). To reconcile these differences between NRD theories and dFe isotope observations, we need to consider any physicochemical partitioning within the dFe pool. The abundance and isotope composition of dFe (<0.2 μm) may reflect variable contributions of mineral or organo-mineral Fe colloids (cFe, 0.02 to 0.2 μm) in addition to any ligand-bound Fe and sFe(II/III) species (<0.02 μm) in the ocean (23, 27). Such components of the dFe pool are often unaccounted for and have been neglected in previous studies reporting the occurrence of sedimentary NRD in the water column. However, sizable concentrations of cFe (10^1 μmoles · L^{-1}) have been observed in oxic-nitrogenous porewaters from deep ocean turbidites of the Southern Ocean, where dFe isotope compositions also matched the solid phase inputs from ocean island basalt. Whether these colloids were formed in situ through organic complexation and/or as secondary minerals from either reductive or nonreductive processes was unresolved. A comparison to fresh tephra layers in the Caribbean Sea showed that ocean island basalt weathering and production of nanoscale ferrihydrite or Fe-bearing smectite clays were thermodynamically plausible explanations for cFe in the Southern Ocean porewaters (28). Recently, Klar et al. (7) looked for Fe colloids in porewaters from a shallow shelf sediment, but found few if any, and that the porewaters were dominated by light dFe isotope signatures and sFe(II) attributable to RD by bacteria. Previous studies have not resolved where or why cFe occurs in sediment porewaters of the continental shelf–slope–basin transition or the extent to which they may influence the inventory and isotope composition of dFe input to the ocean (20, 22). These lessons need to be learned by examining the soluble and colloidal partitioning of dFe in porewaters and comparing them to dFe isotope signatures from a wider range of sedimentary carbon and oxygen regimes in the ocean environment.

Without appropriate simulation of this dFe source, ocean biogeochemical models will fail to represent spatial patterns in dFe flux from the seafloor, the response of these fluxes to changing ocean environments, and their consequences for ocean biogeochemistry. Confounding this issue is the omitted role of advective transport mechanisms, internal waves, and benthic boundary layers that will facilitate exchanges between oxic sediments and the ocean interior (3, 29, 30). To make progress on this important issue, we require new understanding on the mechanisms by which Fe dissolves and is supplied to the ocean by oxic sediments.

Herein, we present findings from surface sediment cores from sites that span the depth and breadth of the Southwest Atlantic Ocean. The UK-led GEOTRACES expedition, GA10W, recovered porewaters in 2011 from the Uruguayan continental shelf and slope, Argentine abyssal floor, and Mid-Atlantic Ridge (*SI Appendix*, Table S1). We report porewater dFe isotope compositions and further evidence of the physicochemical partitioning of dFe between soluble and colloidal size fractions (where cFe = dFe−sFe) at selected locations and depths where porewater inventories of Fe were sufficient to permit these determinations. We apply principles of isotope fractionation and mass balance across the dissolved and soluble size classes to test hypothetical controls on the dFe pool in these porewaters. Our study reveals that oxidizing zones of marine sediments are important regions of nonreductive cFe production derived from lithogenic material, which ultimately determine the dFe inventory and isotope composition supplied to the deep ocean.

Results

South Atlantic Sediment Compositions. Between the deepest abyssal station of GA10W (18) to the shallowest shelf-top station (24), core-top sediments were composed almost entirely of lithogenic material (84 to >99%, Fig. 1; averages from 0 to 5 cmbsf, *SI Appendix*, Table S2)—consistent with continental weathering input and dispersion to the shelf, slopes, and abyssal floor of the Argentine Basin [(cf. Weijer et al. (31)]. Lithogenic material was the second most significant component of core-top material (17%) at the most distal station located on the Mid-Atlantic Ridge, station 8, more than 3,500 km from the continental margin along the path of the South Atlantic Current and above the likely calcite saturation horizon (32). Station 8 was predominantly biogenic carbonate ($CaCO_3$) (82%), with trace amounts (<1%) of biogenic opal, whereas stations 18 to 24 contained at most only modest amounts of opal (up to 14%) and $CaCO_3$ (up to 8%). There was a gradient in total organic carbon (TOC) content from a midslope maximum (3.9%, station 22)—coincident with a midslope peak in pelagic components—down to minimum values on the permeable sandy shelf (0.2%, station 24) and across the basin on the Mid-Atlantic Ridge (0.2%, station 8).

Dissolved Porewater Contents. Porewater O_2 was depleted from bottom water values and was observed to penetrate between 0.4 and >9 cmbsf across all sites. There was a strong exponential relationship between calculated rates of C oxidation (determined from O_2 flux) and water depth (*SI Appendix*, Fig. S1 and Table S3). Other such indicators of early diagenetic cycling in porewaters had equivalent water depth dependence between stations.

Porewater nitrite + nitrate (herein after termed nitrous oxides) was depleted down core from bottom water values (*SI Appendix*, Fig. S2) and coincided with increased ammonia concentrations (*SI Appendix*, Table S4). Taken together, these data indicate the reductive cycling of nitrous oxides to ammonia in a nitrogenous zone underlying the oxic surface layer. All stations contained subsurface maxima in dissolved manganese (dMn) and dFe, up to 10 and 52 μM, respectively, consistent with the RD of these metals that has been observed beneath oxic-nitrogenous zones elsewhere in deep-sea sediments (e.g., refs. 9 and 33). A single exception was station 8, where nitrous oxides were not obviously depleted and where neither dMn nor dFe maxima were observed (*SI Appendix*, Fig. S2 and Table S5).

Porewater δ^{56}Fe of dFe maxima averaged −0.93 ± 0.2‰ (1 SD, $n = 5$) between stations 18 and 24 (*SI Appendix*, Fig. S2) and were isotopically lighter than average igneous crustal material at δ^{56}Fe = +0.09‰ (34). Light dFe isotopic compositions shifted to heavier values down core and exceeded the average isotopic composition of the crust beneath the ferruginous zones of stations 23 and 22 (up to a maximum of +0.63‰). Nearly all stations contained porewater concentrations of dFe in the surface oxic-nitrogenous zones 10 to 500 times higher than background seawater concentrations with δ^{56}Fe (+0.07 ± 0.07‰, $n = 11$) indistinguishable from average crustal rocks. A single exception was station 23, where ferruginous conditions extended into the upper centimeter of the sediment and a light dFe isotope composition were observed (−1.37‰).

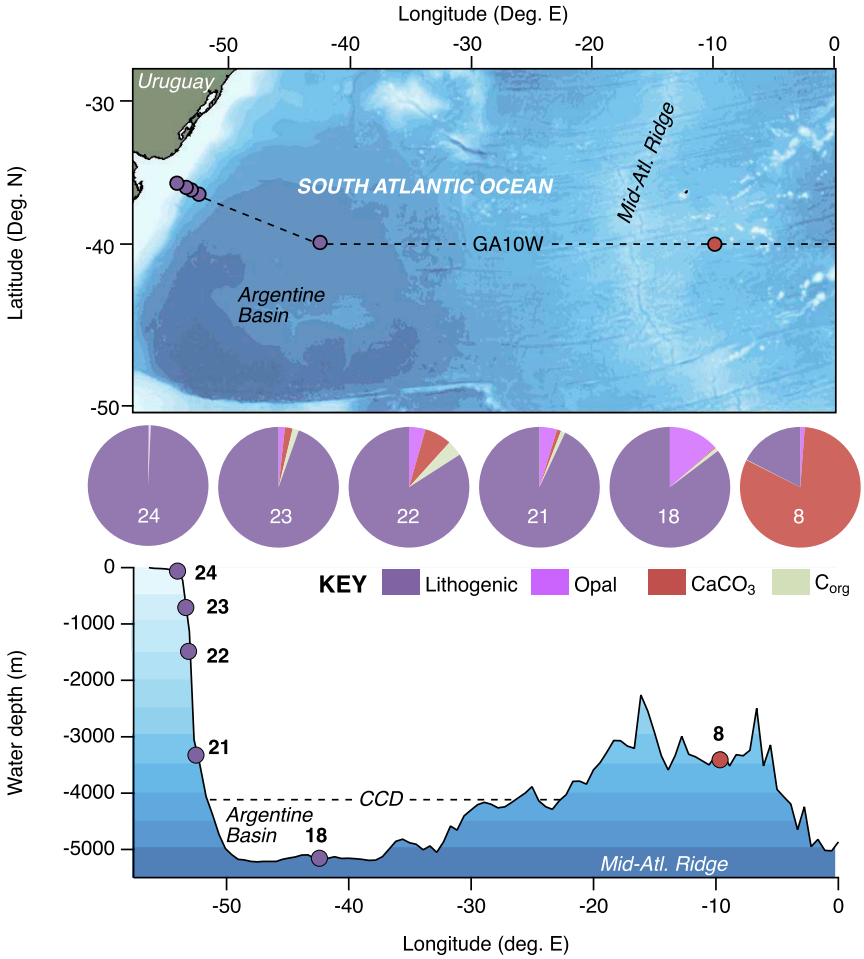

Fig. 1. The location and core-top composition of sediment samples collected from GA10W are shown relative to lattitudinal degrees North, longitudinal degrees East and water depth. A blue color index shows 500 m water depth intervals in a plan view (*Top*) of the study region and a section view (*Bottom*) along the GA10W sample transect. Sediment classifications of stations 8 to 23 include cohesive silts clays, whereas station 24 is a noncohesive permeable sand. Station 18 lies well beneath the likely $CaCO_3$ compensation depth. Pie charts indicate the mean surface (0 to 5 cmbs) proportions of lithogenic and pelagic components between all sites (*SI Appendix*, Tables S1 and S2).

Soluble and Colloidal Partitioning of dFe in Porewaters. A comparison of soluble (<0.02 μm) and dissolved (<0.2 μm) porewater filtrates at stations 8, 18, 21, and 22 indicates that subsurface maxima in dMn and dFe concentration were almost exclusively due to the presence of soluble and most likely reduced species of the metals [Fig. 2 and *SI Appendix*, Table S5; cf. (7)]. However, porewater also contained significant detectible quantities of dFe (between 0.01 and 0.5 μM) that was far in excess of sFe throughout the overlying nitrogenous and oxic zones. Therefore, between 17 ± 6 and 99 ± 3% of dFe in oxic-nitrogenous porewater was in a colloidal size-class (0.02 to 0.2 μm, Fig. 2). To a lesser but significant extent, dMn also occurred as colloids in the oxic porewater (between 0 and 61 ± 5%, *SI Appendix*, Table S5).

Discussion

Early Diagenesis of Fe and Mn. High proportions of lithogenic materials relative to pelagic material on the Uruguayan margin and deep Argentine Basin, compared to the Mid-Atlantic Ridge (Fig. 1), broadly match regional sediment classifications in a recent census of the seafloor, which indicates these sites are also typical of many other margin, basin, and ridge environments of the global ocean (35). Calculated fluxes of O_2 in cohesive sediments from the upper shelf slope (station 23) to Mid Atlantic Ridge (station 8), and the relationship of these fluxes to water depth (*SI Appendix*, Fig. S1), follow an expected gradient in the amount of OC that survives remineralization in the water column and enters the sediment to fuel early diagenetic reactions (36). Porewater properties reported here may therefore provide a suitable analog for other oxygenated shelf–slope–basin transitions of the global ocean.

Porewater concentration profiles provide evidence for a common down-core sequence of electron acceptor cycling in the order $O_2 > NO_x > Mn^{4+} > Fe^{3+} > SO_4^{2-}$, which follows the Gibbs free energy available to the bacteria which catalyze these reduction–oxidation pathways (37). The soluble nature of dFe and dMn maxima (*SI Appendix*, Fig. S2) is evidence for the reduced species of these metals accumulating in porewaters [cf. (7)]. The light isotopic composition of dFe in these ferruginous zones matches previous findings too, in which RD of Fe(III)oxyhydroxides to $sFe(II)_{(aq)}$ was also reasoned to account for similar light $\delta^{56}Fe$ values (5–7, 9, 11, 38, 39), and is supported by experiments (40, 41). However, our investigation of the oxic-nitrogenous zones provides evidence for a previously undocumented reservoir of cFe in continental slope and basin sediment porewater of the South Atlantic Ocean (Fig. 2). These colloids will play a crucial role in regional Fe supply, particularly in deep waters, and their occurrence signifies that they are likely to be prevalent in other oxygenated slope and basin environments.

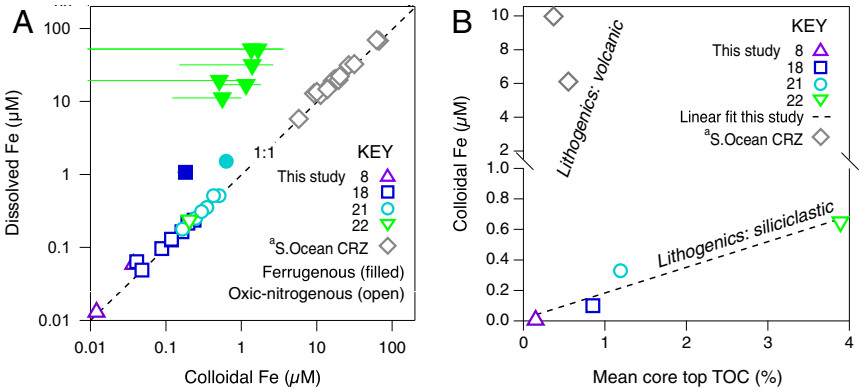

Fig. 2. (*A*) Porewater concentrations of dFe versus cFe. Error bars (±2 sigma) are typically within the size of individual data markers. Discrete observations from oxic-nitrogenous zones fall along a 1:1 line due to the high relative abundance of cFe. The concentration of dFe exceeds cFe concentrations in underlying ferruginous zones due to the low relative abundance of cFe in these regions of the sediment. Concentrations of cFe span three orders of magnitude in porewater oxic-nitrogenous zones across all sites and exceed the concentrations of ocean bottom water (24). (*B*) Mean porewater cFe concentration versus mean TOC in core-top sediments (0 to 5 cmbsf). A dashed black line shows a significant linear fit through GA10W sites ($r = 0.962$, $P = 0.038$). (a) Values from mafic volcanic sediments in the Southern Ocean near the Crozet Islands (S.Ocean CRZ) (28) indicate that additional factors other than TOC also control the abundance of cFe in porewater, such as lithogenic provenance.

The Occurrence of Fe Colloids in Sediment Porewater. Iron colloids occur commonly in the ocean (23, 27, 42). Most often they are attributed to organic complexation of Fe(III) (43, 44), nanoparticulate Fe(oxyhdr)oxide, clay (45–47), or occasionally Fe-sulphide (48) minerals. Recent findings indicate deep Atlantic Ocean waters contain cFe that originates from the seafloor (27), but there are comparatively few assessments of cFe in marine sediment porewaters beyond those presented and discussed in this article (6, 7, 28).

Our study shows that the occurrence of cFe in surface sediment porewater is extensive and, thus far, ubiquitous in oxic deep-ocean lithogenic sediments. What is more, these colloids share a nearly identical Fe isotope composition throughout the ocean: In porewaters, where dFe has been shown to comprise between 70 and 100% cFe, the dFe isotope composition (+0.12 ± 0.07‰, $n = 24$) remains indistinguishable from the δ^{56}Fe of the average igneous weathering product [+0.09‰ (34); Fig. 3]. It stands to reason that a common mechanism must be responsible for the formation of cFe from lithogenic material in oxidizing environments, which can operate independently of RD driven by bacteria to account for this isotopic uniformity between cFe and lithogenic materials.

The Fe isotope composition of igneous rocks is reflected in its detrital weathering and oxidation product (49, 50). We expect sediments derived from different igneous rocks with different histories of siliciclastic cycling to exhibit variable rates of seafloor weathering, dissolution, and authigenesis (3, 9, 51, 52). Accordingly, the porewater content of cFe reported from young deep-ocean Crozet Islands basalt is greater than we report here for the South Atlantic, even for basaltic sites with comparatively low TOC (Fig. 2*B*). In the present study, however, between sites that share a similar lithogenic provenance, we see a strong positive correlation between mean cFe concentration in oxidizing porewater and the mean core-top abundance of TOC ($r = 0.962$, $P = 0.04$, $n = 4$; Fig. 2*B*). Taken together, these igneous and organic relationships reinforce the view that cFe is controlled by the weathering of lithogenic detritus and that OC may be required for the stabilization of cFe we observe in the porewaters. For example, OC sorption to oxyhydroxide mineral surfaces can inhibit Fe transformation into more crystalline and refractory minerals. This interaction is evidenced experimentally (53) and by observations that show that one fifth of marine sedimentary OC is bound to reactive Fe phases (54), which are predominantly nanoscale oxyhydroxides in marine sediment oxic layers (47). Therefore, Lalonde et al.'s (54) proposition of a "rusty sink," in which formation of metastable Fe(III) organo-minerals promotes OC burial, may here prove to be a "rusty source" mechanism for the occurrence of cFe in oxic porewater. In other words, our assessment of core-top TOC and cFe content could reflect the availability of OC compounds formed during organic matter degradation and that are suited to stabilization of nanoscale Fe oxyhydroxide.

Mechanisms Governing the Production of Porewater Fe Solutes and Mineral Colloids. It is important to determine whether cFe in oxidizing porewater is an authigenic precipitate of Fe produced by RD or if it has formed by a distinctly nonreductive pathway because these processes of colloid production (or within our

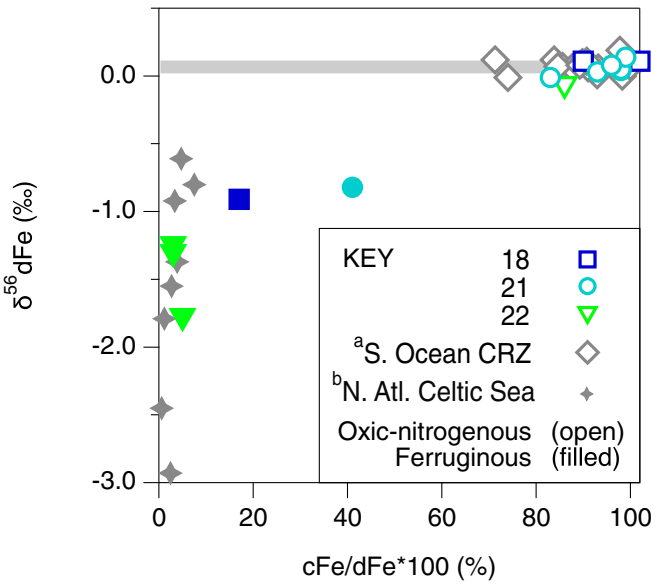

Fig. 3. The relationship between δ^{56}dFe and relative abundance of cFe in ocean sediment porewater. Values compiled from the South Atlantic (this study sites 18, 21, and 22) and previous studies by (a) Homoky et al. (6) and (b) Klar et al. (7). Error bars (±2 sigma) are within the size of individual data markers. The gray bar indicates the average Fe isotopic composition of crustal rocks.

operational definitions here, sediment dissolution) will have different drivers and impacts in the ocean and may respond and feed back differently to changes in the overlying ocean environment. Addressing this issue is essential if we are to build confidence in the paradigms, we depend upon to estimate the size and variability of iron inputs in ocean biogeochemical models (3, 4, 18).

We can simulate the steady-state porewater production/consumption profiles needed to reproduce measured soluble, dissolved, and colloidal Fe concentration profiles across an oxic-nitrogenous zone. Of the GA10W transect, station 21 offers uniquely detailed data resolution to perform this assessment with the one-dimensional steady-state "Rate Estimates from Concentration profiles" or REC model previously described by Lettman et al. (55). If we impose a lower boundary condition for sFe and dFe concentrations equal to porewater maxima at 8.5 cmbsf, and a surface boundary condition of 1–10 nmol $\cdot$ L^{-1} to approximate bottom water (24), model fits to sFe and dFe data (and cFe by difference) may be calculated (Fig. 4 and *SI Appendix*, Table S6).

The sFe profile is reproduced with a single region of production in the ferruginous zone (>7.5 cmbsf) and a single region of consumption above it (5 to 7.5 cmbsf) in accordance with the oxidizing potential of nitrous oxides. A more complex production profile is required to simulate dFe, which is predominantly determined by the production of cFe rather than sFe. Production of cFe coincides with a region of sFe consumption (between 5 and 7.5 cmbsf), indicating sFe-oxidation could partially contribute an authigenic source to cFe in porewater. However, the dFe profile requires similar magnitudes of cFe production in oxic, nitrogenous, and ferruginous zones. Therefore, sFe oxidation alone does not fully account for the production of cFe.

Porewater Isotopic Constraints on the Genesis of cFe. We can further test hypothetical controls on the genesis of cFe using an isotopic mass balance model. We consider two scenarios in which the isotopic composition of dFe is determined by theoretical controls on soluble and cFe species: In the first scenario, sFe [assumed here to be $Fe(II)_{aq}$] is oxidized and isotopically fractionated, and cFe is assumed to form entirely from the authigenic products of sFe oxidation. In the second scenario, sFe is oxidized and isotopically fractionated, but removed to the sediment, and cFe is formed entirely from the oxidative weathering of lithogenic material without any Fe isotope fractionation. Initial isotope ratios for sFe and cFe can be adjusted so that the resultant dFe isotope ratio matches the observed value at the dFe maxima 9.5 cmbsf. The isotope compositions of sFe and authigenic cFe can then be determined by an isotope fractionation factor (α) during $Fe(II)_{aq}$ oxidation. Herein, we choose to evaluate values of α <1 and >1, where $\Delta_{sFe\text{-}cFe}$ was ±0.5‰ (*SI Appendix*, SI Text S2).

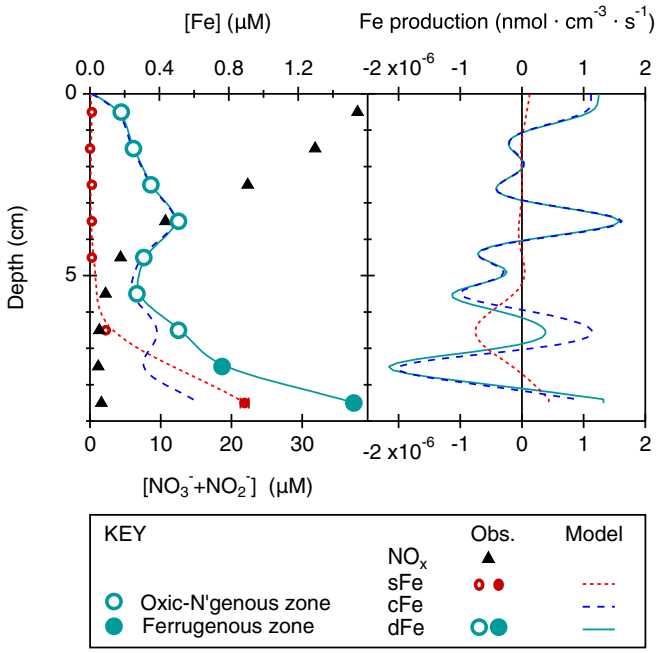

Fig. 4. Modeled porewater Fe production rate profiles. The comparison of measured sFe and dFe with rate estimates from concentration model fits to observations across the oxic/nitrogenous-ferruginous transition of GA10W station 21. The concentrations and production rates of cFe are calculated by model difference (cFe = dFe−sFe).

By modeling these idealized controls on the isotopic composition of porewater dFe, we make two interesting observations. Firstly, porewater dFe isotopes cannot be reproduced when oxidation of sFe determines the isotope composition of cFe (Fig. 5 *A* and *B*), whereas dFe isotopes are reproduced quite well when cFe reflects a homogenous crustal weathering product (Fig. 5 *C* and *D*). Secondly, dFe isotopes are most accurately reproduced at the transition between ferruginous and oxic-nitrogenous conditions (i.e., region of maximum sFe consumption; cf. Fig. 4) when α is <1. We achieve our best simulation of porewater dFe isotopes when cFe is lithogenic and sFe is consumed by oxidation with α of 0.9995 (Fig. 5*D*).

We note that the nature of authigenic mineral sinks linked to sFe oxidation will be more complex than has been represented in our simplified approach to isotopic mass balance above. For example, sFe oxidation may be catalyzed by NO_3-reducing Fe(II)-oxidizing bacteria—most prevalent in marine sediments with low to moderate TOC content (56). Siderite [$Fe(II)CO_3$] is also a common authigenic precipitate of $Fe(II)_{aq}$ that produces kinetic and equilibrium isotope effects [$Fe(II)_{aq}$-$FeCO_3$ = Δ +1.2 and 0.0‰, respectively (57)].

Crucially, however, authigenic Fe minerals must either preserve or fractionate isotope ratios from their source of aqueous Fe(II). If Fe(II) is produced from ferruginous depths in porewater following conventional RD theory, then any such authigenic minerals must either preserve [e.g., via $Fe(II)CO_3$] or fractionate (e.g., via oxidation to ferrihydrite) the light isotope composition of the Fe(II) supplied from the ferruginous zone. Because we have chosen to consider a range of α values (from 0.9995 to 1.0005), our simulations may represent a wide range of potential isotope fractionations that might reasonably be achieved by formation of common authigenic Fe minerals (40, 41, 57, 58) or by complexation of sFe with organic ligands (26, 50). Yet we still determine cFe isotopes to be almost uniformly identical to the continental crust, within and between ocean basins. This occurs in the presence of contrasting sediment composition (e.g., opaline, $CaCO_3$, basaltic, siliciclastic, and TOC content) between sites. Such compositional variability would theoretically encourage variations in the solubility of different authigenic phases and therefore impart different isotope fractionation effects upon $Fe(II)_{aq}$ between sites, but this variability in the cFe pool is simply not observed (Fig. 3). For these reasons, we consider that cFe is principally formed by oxidative weathering of lithogenic material without dissimilatory reduction and isotope fractionation by bacteria. While bacterial siderophores may promote Fe oxide and Fe-bearing silicate mineral dissolution, they can do so indirectly via proton-promoted dissolution (59), which does not fractionate Fe isotopes (60). We posit that nanoscale ferrihydrite produced by oxidative weathering is further stabilized by the sorption of OC, but sorption to the Fe mineral surface imparts no fractionation effect and therefore preserves its Fe isotope composition.

Implications for the Ocean Fe Inventory. A lithogenic source of Fe colloids in surface oxidizing porewater has important implications for our assessment of benthic Fe supply to the ocean.

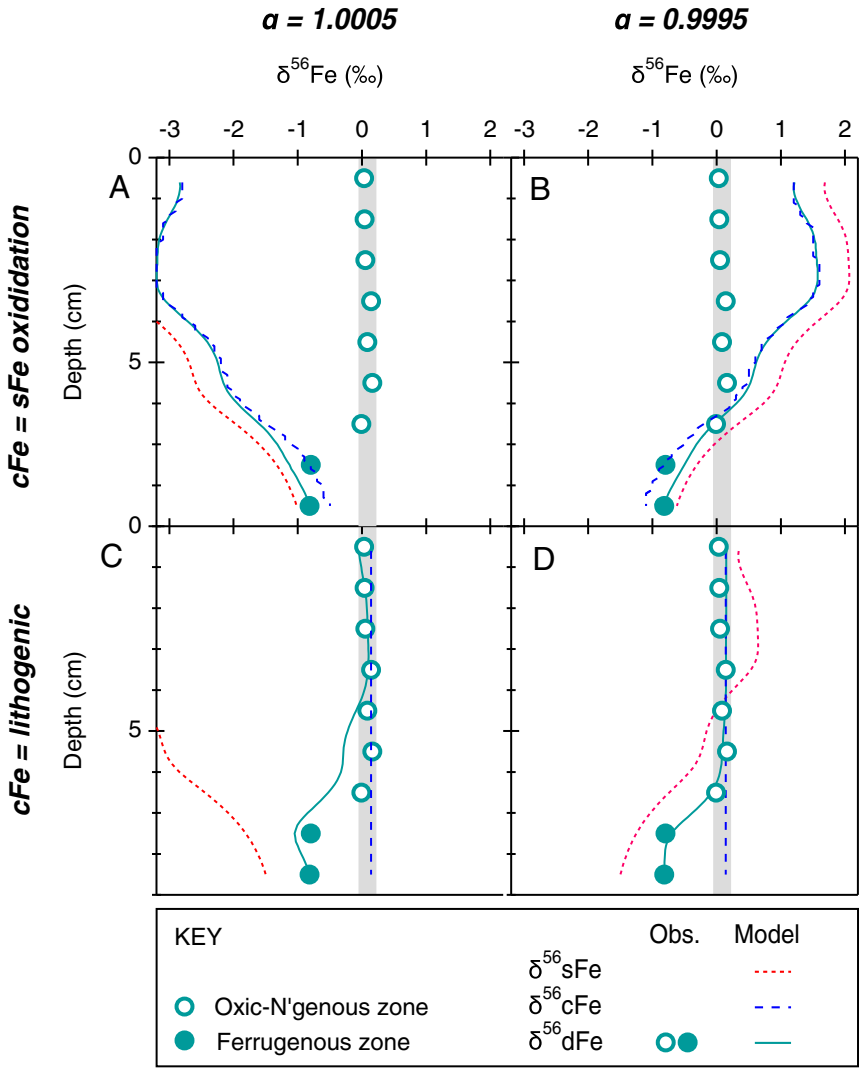

Fig. 5. Porewater sFe and cFe isotope mass-balance experiments. The summary of results in which porewater dFe isotope compositions are simulated by two idealized controls on the sFe and cFe isotope reservoirs: Firstly, the isotope fraction effect (α) attributed to sFe loss (e.g., oxidation) and secondly, the origin of porewater cFe. The value of α is either >1 (*A* and *C*), as is commonly predicted for Fe(oxyhydr)oxide formation or <1 (*B* and *D*) and has been attributed to Fe (oxyhydr)oxide formation across some ocean chemoclines (15), or is predicted by some other (e.g., $CaCO_3$) mineral formations (57) and Fe(III)-ligand complexes (26). Porewater cFe is either an authigenic mineral supplied by sFe oxidation with a corresponding isotope composition (*A* and *B*), or cFe is supplied by nonreductive weathering of lithogenic material with crustal isotope compositions (*C* and *D*). In all scenarios, the resultant composition of dFe reflects the isotopic mass balance of sFe and cFe pools. Model equations are provided in *SI Appendix*, SI Text S1.

The oxidizing conditions we find supporting cFe production reported here reflect those that occur commonly below the sediment–water interface of major open ocean margins and basins (36). Thus, we provide key porewater evidence to refute the assumption that only RD controls benthic input of dFe to the ocean (8, 9). Organo-mineral Fe weathering products with a longer oceanic residence time than reduced-Fe species may also explain how dFe bearing nonreductive crustal isotopic signatures can escape the seafloor and be transported to the ocean interior.

The resultant flux of lithogenic Fe colloids to the ocean will reflect the balance of in situ production rates and benthic exchange mechanisms (Fig. 6). We find that the absolute abundance of cFe in porewater remains greatest in sediments composed of fresh basaltic weathering products, likely indicative of the higher Fe and Mn contents of mafic source rocks and the susceptibility of mafic minerals (e.g., basalt glass, olivine, and amphibole) to weather rapidly and produce Fe(oxy)hydroxides and clays during marine early diagenesis (cf. Fig. 2*B*). We also find that OC is an important additional factor in the production of cFe, but we can only speculate as to the nature of OC moieties in porewater that might elicit the strong cFe relationship with TOC observed in South Atlantic sediments. We suggest that degradation of organic matter may yield bacterial communities and compounds with functional groups suited to 1) enhance the oxidative weathering Fe oxide and Fe-bearing silicate minerals (59) and 2) the sorption of Fe(oxyhy)oxides present in oxic zones (61), which inhibits the loss of Fe to more crystalline phases and encourages preservation as nanominerals (54). If so, then seafloor OC supply may still exert an important overarching influence on sedimentary dFe fluxes to the ocean, only here it is due to enhanced NRD and mineral-protection effects, rather than RD or ionic complexation processes that fractionate Fe isotopes (5, 26).

Benthic exchange mechanisms will promote the flux of cFe produced by seafloor weathering and OC complexation to the ocean interior (Fig. 6). Established gradients in cFe concentration between porewater and bottom water may promote a diffusive flux of colloids toward the deep ocean. Without knowledge of cFe diffusion coefficients, diffusive flux calculations may inaccurately

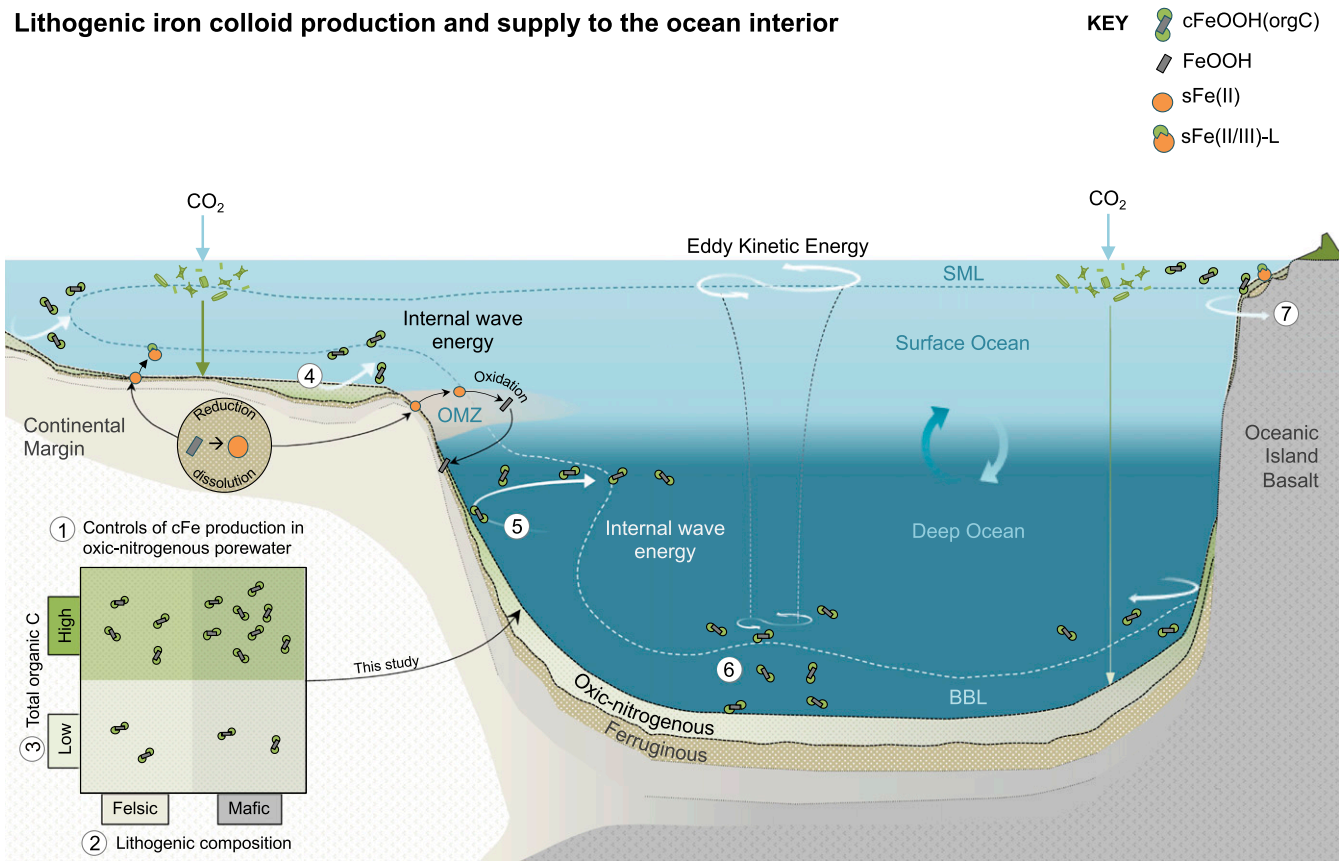

Fig. 6. A revised scheme of sedimentary iron supply depicting seven processes that may promote the exchange of lithogenic cFe and isotopes to the ocean interior. 1) The production and diffusion of cFe [depicted as cFeOOH(orgC)] in oxic-nitrogenous ocean sediment porewater; 2) enhanced cFe production from dissolution of mafic minerals; 3) enhanced cFe stabilization by organic C; 4) porewater advection through permeable sediments of the continental shelf (70); 5) entrainment by internal waves and density horizons (16); 6) entrainments by a benthic boundary layer (BBL) coupled to surface ocean eddy kinetic energy (29); and 7) entrainment by the surface mixed layer (SML) and island mass effects (71). The sedimentary release of sFe by RD is restricted to shoaled porewater ferric lines beneath high organic matter flux or oxygen minimum zones (OMZs) in the upper 1,500 m of the ocean and rely on stabilization by organic ligands to resist secondary oxidation and precipitation from the water column (7, 12, 16).

need to assume their behaviors match those of the aqueous ion. On the other hand, the stability of organo-mineral colloids in the presence of oxygen means that large reactive losses, such as those required to account for oxidation of aqueous Fe(II) (7, 12), may not be applicable to an assessment of cFe (28). Of further significance, biophysical activity and bottom shear stress will promote the entrainment of surface sediment and porewaters in the ocean (46, 62). These entrainments can encourage the scavenging removal of aqueous Fe(II) and Fe(III) species present in excess of ligand concentrations (e.g., ref. 12) and simultaneously promote the exchange of mineral solids (including colloids) between the sediments and the water column (27, 29). Energy for the generation and transport of a benthic nepheloid inventory appears unevenly in the ocean. It is tied to upper-ocean dynamics and the internal tide and is compounded by bathymetric roughness, island mass effects, and reflection angles (29, 63, 64). Despite complexity to these interactions, their importance for boundary exchange and transport in the ocean is well recognized (16, 30) and even evidenced to facilitate the supply of cFe (23, 27) and lithogenic Fe isotopes to the water column (20) (Fig. 6).

Where sites of maximum cFe production and potential benthic entrainment overlap, conditions suited to produce a flux of cFe and crustal isotope signatures to the ocean ought to be optimized (Fig. 7). Improved knowledge of where cFe fluxes occur would assist their inclusion in new generations of ocean iron cycle models, which would, in turn, provide an opportunity to update our understanding of how sedimentary iron supply impacts the ocean carbon cycle (2). Optimal conditions for sedimentary cFe input in the ocean may be predicted, firstly, by considering the known surface exchangeable (0 to 1 cmbsf) inventory of porewater Fe-bearing crustal isotope compositions (Fig. 7*A*). Large differences exist in the dFe isotopic signature of surface exchangeable porewater in the upper 1,500 m of the ocean with a tendency toward light values that are attributable to the variable influence of reductive and nonreductive sediment dissolution. By contrast, the isotopic signatures from equivalent porewater depths are far more uniform and crustal in ocean sediments beneath 1,500 m due to the lithogenic production of cFe in oxic-nitrogenous zones. These sites also correspond to low-benthic oxygen consumption rates (<2 mmol $\cdot$ m^{-2} $\cdot$ d^{-1}) sufficient to suppress the generation of sFe by RD in ferruginous zones well below the sediment–water interface. Secondly, the entrainment potential for cFe is illustrated by comparing compilations of benthic O_2 flux [sediment community O_2 consumption rates (65)] and the benthic nepheloid inventories observed in bottom water (29) (Fig. 7*B*). Sediments below 1,500 m water depth exhibit the lowest rates of O_2 consumption, almost exclusively <2 mmol $\cdot$ m^{-2} $\cdot$ d^{-1}, so that they are most likely to contain exchangeable porewater inventories of lithogenic cFe (cf. Fig. 7*A*). Bottom waters bearing the highest benthic nepheloid inventories are also found in deep waters, notably in western margins and basins of the North and South Atlantic Ocean, indicating that these regions could optimize the entrainment

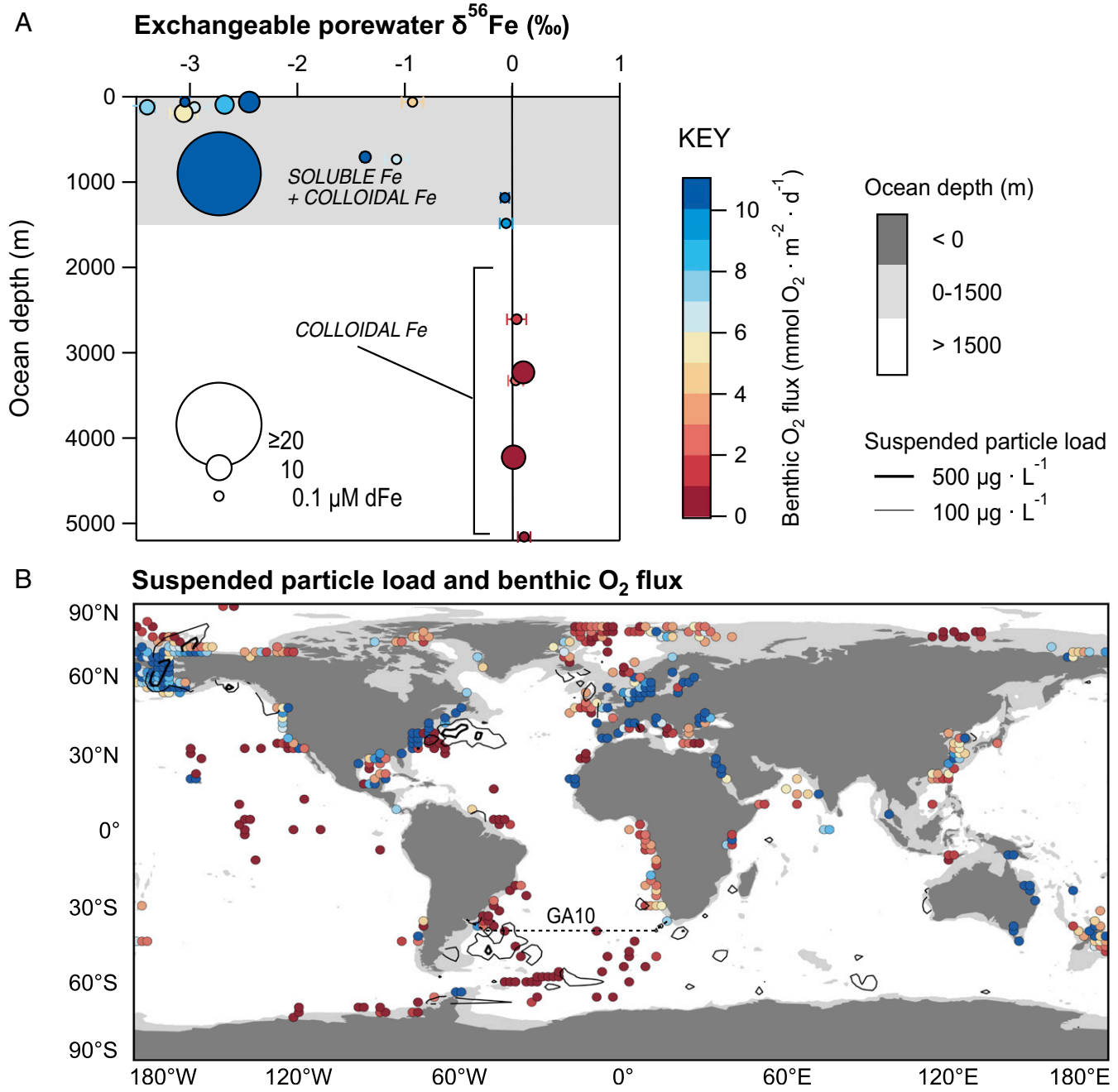

Fig. 7. (*A*) The isotopic signature of dFe in surface exchangeable sediment porewaters. Data markers correspond to the measured surface values compiled from this study (*SI Appendix*, Table S5), the South Atlantic, Cape margin (9), North Pacific, Oregon and California margins, Borderland Basins (6, 11), North Atlantic, Celtic Sea (7), Southern Ocean, and Crozet Islands' abyss (6). The measured surface inventory of porewater dFe is illustrated by the size of data markers, and the associated benthic flux (sediment consumption) of O_2 is illustrated by the color scale. (*B*) The entrainment potential for cFe and lithogenic isotope signatures in the ocean. The mean sediment community O_2 consumption rates complied by Stratmann et al. (65) are gridded here at 2° and plotted using the same color scale to data in *A*. The suspended particle load in bottom waters reported by Gardner et al. (29) is reproduced with interpolated lines of equal concentration using means values from a 2° grid.

of cFe and lithogenic isotopes in the ocean. Shelf and slope sediments above 1,500 m show the highest benthic fluxes of O_2, consistent with these regions supporting reservoirs of reduced, soluble, and light Fe isotopes in porewaters that can be exchanged with the upper ocean (7, 11). A high degree of variation to benthic nepheloid inventories and oxygen flux (<1 to >10 mmol $\cdot$ $m^{-2} \cdot d^{-1}$) is also shown in sediments above 1,500 m (Fig. 7*B*) and suggests the relative contributions of RD and NRD might vary considerably between regions of the upper ocean.

Furthermore, localized and seasonal variations in sediment dissolution and mechanisms of entrainment are certain to exist, particularly close to margins, that are not represented by the data or grid resolution presented here. The exchangeable inventories of cFe in oxidizing porewaters will also respond to the underlying influence of igneous provenance and OC (cf. Fig. 2*B*), which we have not explicitly accounted for. Therefore, the broader implications of our findings are potentially significant but not yet known. The stability of organo-mineral Fe colloids means they

may not succumb to the same fate (rapid precipitation, aggregation, and removal) that limits the extent to which reductive Fe inputs influence the ocean interior. By the same token, the bioavailability of these organo-mineral Fe colloids is unknown and begs the question: Is there a trade-off between the endurance of Fe colloids in the ocean and their accessibility for phytoplankton? An additional, more stable source of dFe deeper in the water column governed by lithogenic colloid production, which has been ignored in our earlier numerical and conceptual models of the iron cycle, will contribute to the buffering of the ocean dFe inventory against variability from other sources and further lower the mean residence time of dFe.

Conclusions

South Atlantic sediments contain a nonlinear down-slope gradient in O_2 consumption rates, with coupled porewater depth zonation of nitrous oxide, Mn oxide, and Fe oxide reduction pathways, which are consistent with anticipated down-slope gradients in OC flux and decomposition at the ocean floor. Porewater maxima in dFe contents have light Fe isotopic composition in the form of mostly sFe species, reflecting the RD of Fe(III) to Fe(II) by bacteria in ferruginous zones. Beneath these maxima in dFe contents, heavy dFe isotopes corresponded to the reactive loss of sFe(II) with free sulphide. Detectable amounts of dFe in the overlying oxic-nitrogenous zones have dFe isotope compositions that are indistinguishable from average igneous weathering products due to the production of Fe colloids from lithogenic weathering. Based on a strong correlation between cFe abundance and TOC, we propose cFe stability may be promoted by Fe(oxyhydr) oxide adsorption to OC and the formation of nanoscale ferrihydrite organo-mineral composites.

Modeled porewater production and consumption profiles indicate that a sFe pool of Fe(II) accounts for the light isotopic composition of ferruginous zones, whereas dFe and its isotope composition was mostly determined by the genesis of cFe in overlying oxic-nitrogenous zones of marine sediments. Our isotopically constrained model experiments show that nonreductive weathering of lithogenic material is required to account for the widespread occurrence of cFe in porewater—oxidative conversion of sFe(II) to cFe(III) alone—was an insufficient explanation for the presence of Fe colloids and their isotope composition, as were alternative authigenic mineral or ligand-stabilized "sinks" for sFe(II) supplied by RD.

We determine that oxic-nitrogenous ocean sediments support lithogenic weathering and organo-mineral formation, and may provide a "rusty source" of cFe throughout the global ocean. Coupled to the generation of benthic nepheloid inventories, oxidizing sediments will be important sites for benthic Fe exchange that need to be reappraised for their role in ocean biogeochemical cycles.

Materials and Methods

A Bowers–Connelly Mega Corer collected multiple intact surface sediment cores from six sites in the South Atlantic during occupation by the Royal Research Ship James Cook (JC068) in 2011. All cores were transferred to a controlled temperature laboratory replicating bottom water conditions (4 to 8 °C) for microsensor profiling, porewater extraction, and solid sampling, in which all apparatus in contact with the samples (syringes, Teflon, centrifuge tubes, and low-density polyethylene) and bottles were cleaned prior to use (72 h in 10% Decon, 72 h in 6M HCl, 72 h in 6M HNO_3, and rinsed by 18.2MΩ deionized water).

Microsensor determinations of dissolved oxygen were performed by a Unisense microprofiling suite of apparatus following analytical procedures previously described and used in coastal and deep-sea sediments elsewhere (7, 9, 28). Oxygen penetration depths were either measured directly in the upper 6 cm or estimated from model fits to steady state oxygen consumption rates as previously described (7, 9). Core-top physical properties were assessed on the same core used for oxygen profiling. Porosity and dry-bulk density were determined from the difference between wet mass and salt-corrected dry mass of 10 mL sub-samples at 2 cm depth intervals.

Rhizon samplers (2.5 × 50 mm "CSS" type, Rhizosphere Research Products) were inserted at 1–2 cm depth intervals through predrilled holes into a second sediment core recovered from the Mega Core deployment. Porewater was filtered (~0.15 μm) by suction through each Rhizon into a BD Discardit syringe in an ambient atmosphere. Sample aliquots (2 mL) were diluted 15-fold by 18.2 MΩ deionized water and stored in the dark prior to ship-board nutrient analyses (NO_3^-, NO_2^-, and NH_4^+) by a five-channel Bran and Luebbe AAIII segmented flow colorimetric auto analyzer after Homoky et al. (9) and previously reported by Bridgestock et al. (66).

Under a nitrogen atmosphere, a third sediment core was extruded, sliced at 1–2 cm depth intervals, and centrifuged at 9,000 g for 6 min before supernatant porewaters were siphoned through Teflon tubes into BD Discardit syringes. Samples for dissolved metals were passed through Whatmann Puradisc 25 syringe filters with polyethersulphone membranes (0.2 μm) and selected subsamples for soluble metals were passed through a second, in-line Whatman Anatop 25 syringe filter with aluminum oxide membrane (0.02 μm). All porewater samples were later acidified to pH < 2 by adding 6 μl of 6M quartz distilled HCl per milliliter of sample and stored refrigerated prior to analyses.

Sediment residues from centrifugation were freeze dried under vacuum and later pulverized in an agate pestle and mortar for carbon and opal determinations. The bulk composition of sediment cores is described by dry-mass measurements of the total $CaCO_3$, TOC, opal, and—by difference from the total dry mass—lithogenic material. The difference between coulometric determination (UIC 5012 Coulometer) of total carbon (TC) and total inorganic carbon (TIC) content of powdered sediments were used to calculate TOC. TC was calculated from CO_2 released during sample combustion, and TIC was calculated from CO_2 released during heated sample reaction with 1.5 M H_3PO_4. Accuracy of TC and TIC determinations was assessed with anhydrous $CaCO_3$ powder, with a mean recovery of 100.4 ± 0.8% (1SD, $n = 15$). The limit of detection (3SD of blanks) was 10 mg C, equivalent to 0.03 wt% TOC. Opal content was measured by molybdate blue spectrometry on Si extracted solutions from dry homogenized sediments following the sodium bicarbonate sequential leaching method according to Mortlock and Froelich (67). Accuracy of opal determination was assessed by multiple analyses of a laboratory bulk sediment at the School of Geosciences, University of Edinburgh with a reproducibility of 1.54%.

A Thermo Scientific element ×2 inductively coupled plasma-mass spectrometer was used to determine the concentration of aqueous metals in acidified porewater samples and sediment digests following Homoky et al. (9) and previously reported by Bridgestock et al. (66). Briefly, porewaters were diluted 100-fold with 0.48 M Q-HNO_3, and external calibration standards were matrix matched to samples with 1% of the certified reference seawater standard NASS-5 (National Research Council of Canada). The mass of ^{45}Sc spiked to all samples was used as an internal standard to monitor and correct for a reduction in signal intensity of over time. Accuracy of the method was verified by the intermittent analysis of a blank-bracketed certified reference riverwater standard SLRS-5 (National Research Council of Canada) within certified values, with a relative SD of 1.1 and 1.3% for Fe and Mn, respectively. The limit of detection (3SD of analytical blanks, $n = 9$) for reported Fe and Mn were 1 and 0.1 nmol · l^{-1}, and procedural blanks were below these limits of detection.

The dFe isotopic compositions from porewaters were measured following previously published methods (9, 68). Aliquots of porewater containing Fe inventories from 20 to 104 ng were spiked with an ^{57}Fe-^{58}Fe double spike (in a 1:2 sample:spike ratio), evaporated to dryness in 7 mL Savillex PFA Teflon vials, and then redissolved in 5 M quartz-distilled HCl + 0.001% (by volume) Optima H_2O_2 before being passed through 135 μL of the analytical grade anion exchange resin AG MP-1 (Bio-Rad) for column purification. Fe was eluted from the columns in 0.8 mL of 1 M quartz-distilled HCl and evaporated to dryness before being redissolved in 0.5 mL of 0.1 M Teflon-distilled HNO_3 for analysis by Multi Collector (MC)-ICPMS. Procedural blanks for this method have previously been shown to be 3 ng of Fe per sample (9). Samples were then analyzed for Fe isotopic composition by Thermo Neptune MC-ICPMS with jet interface at the University of South Carolina, using an ESI Apex-Q introduction system, Pt Jet, and Al X cones, following methods identical to those described previously (9). Fe isotopic compositions ($\delta^{56}Fe$) are expressed in typical delta notion relative to the Institute for Reference Materials and Measurements' international Fe standard IRMM-14. The accuracy of this procedure has been previously demonstrated on seawater samples (68, 69) and here we assign 0.05‰ as an estimate of external precision of analysis, based on duplicate measurements of 60 GA10 seawater samples (0.1 to 1.8 nmol · kg^{-1}), measured over multiple analytical sessions during the same time interval (69). In cases in which the two standard

internal errors are larger than 0.05‰, we consider the 2SE a more representative estimate of uncertainty.

Data Availability. All study data are included in the article and/or supporting information.

ACKNOWLEDGMENTS. We thank the captain and crew of the RRS James Cook expedition JC068 and the science party of UK-GEOTRACES GA10W, in particular, Deborah Hembury and Yu-Te Hsieh (University of Oxford) for shipboard sampling assistance, Malcolm Woodward (Plymouth Marine Laboratory) for shipboard nutrient analyses, and Alex Thomas (University of Edinburgh) for supporting opal analyses by F.D. R.A.M. supported W.B.H. in the collection of sediments and porewater and analyses of oxygen, metals, and carbon through UK Natural Environment Research Council (NERC) Grants NE/F017197/1 and NE/H004394/1. W.B.H. was independently supported by an NERC fellowship at the University of Oxford (NE/K009532/1) to prepare samples for Fe isotope analyses and perform model experiments, and by a University Academic Fellowship at the University of Leeds to write the manuscript. Fe isotope analyses by T.M.C. and S.G.J. were supported by the University of South Carolina. D.K. and A.T. were funded by the European Research Council under the European Union's Horizon 2020 research and innovation program (Grant Agreement 724289).

1. V. A. Elrod, W. M. Berelson, K. H. Coale, K. S. Johnson, The flux of iron from continental shelf sediments: A missing source for global budgets. *Geophys. Res. Lett.* **31**, L12307 (2004).
2. A. Tagliabue, O. Aumont, L. Bopp, The impact of different external sources of iron on the global carbon cycle. *Geophys. Res. Lett.* **41**, 920–926 (2014).
3. W. B. Homoky *et al*., Quantifying trace element and isotope fluxes at the ocean-sediment boundary: A review. *Philos. Trans. A Math. Phys. Eng. Sci.* **374**, 20160246 (2016).
4. A. Tagliabue *et al*., How well do global ocean biogeochemistry models simulate dissolved iron distributions? *Global Biogeochem. Cycles* **30**, 149–174 (2016).
5. S. Severmann, C. M. Johnson, B. L. Beard, J. McManus, The effect of early diagenesis on the Fe isotope compositions of porewaters and authigenic minerals in continental margin sediments. *Geochim. Cosmochim. Acta* **70**, 2006–2022 (2006).
6. W. B. Homoky, S. Severmann, R. A. Mills, P. J. Statham, G. R. Fones, Pore-fluid Fe isotopes reflect the extent of benthic Fe redox recycling: Evidence from continental shelf and deep-sea sediments. *Geology* **37**, 751–754 (2009).
7. J. K. Klar *et al*., Stability of dissolved and soluble Fe(II) in shelf sediment pore waters and release to an oxic water column. *Biogeochemistry* **135**, 49–67 (2017).
8. A. Radic, F. Lacan, J. W. Murry, Iron isotopes in the seawater of the equatorial Pacific Ocean: New constraints for the oceanic iron cycle. *Earth Planet. Sci. Lett.* **306**, 1–10 (2011).
9. W. B. Homoky, S. G. John, T. M. Conway, R. A. Mills, Distinct iron isotopic signatures and supply from marine sediment dissolution. *Nat. Commun.* **4**, 2143 (2013).
10. I. Rapp *et al*., El Niño-driven oxygenation impacts Peruvian shelf iron supply to the South Pacific ocean. *Geophys. Res. Lett.* **47**, e2019GL086631 (2020).
11. S. Severmann, J. McManus, W. M. Berelson, D. E. Hammond, The continental shelf benthic iron flux and its isotope composition. *Geochim. Cosmochim. Acta* **74**, 3984–4004 (2010).
12. W. B. Homoky *et al*., Dissolved oxygen and suspended particles regulate the benthic flux of iron from continental margins. *Mar. Chem.* **134-135**, 59–70 (2012).
13. S. G. John, J. Mendez, J. Moffett, J. Adkins, The flux of iron and iron isotopes from San Pedro Basin sediments. *Geochim. Cosmochim. Acta* **93**, 14–29 (2012).
14. A. Noffke *et al*., Benthic iron and phosphorous fluxes across the Peruvian oxygen minimum zone. *Limnol. Oceanogr.* **57**, 851–867 (2012).
15. M. Staubwasser, R. Schoenberg, F. von Blanckenburg, S. Krüger, C. Pohl, Isotope fractionation between dissolved and suspended particulate Fe in the oxic and anoxic water column of the Baltic Sea. *Biogeosciences* **10**, 233–245 (2013).
16. P. J. Lam, M. I. Heller, P. E. Lerner, J. W. Moffett, K. N. Buck, Unexpected source and transport of iron from the deep Peru Margin. *ACS Earth Space Chem.* **4**, 977–992 (2020).
17. F. Scholz, S. Severmann, J. McManus, C. Hensen, Beyond the Black Sea paradigm: The sedimentary fingerprint of an open-marine iron shuttle. *Geochim. Cosmochim. Acta* **127**, 368–380 (2014).
18. A. W. Dale *et al*., A revised global estimate of dissolved iron fluxes from marine sediments. *Global Biogeochem. Cycles* **29**, 691–707 (2015).
19. J. J. Middelburg, K. Soetaert, P. M. J. Herman, Empirical relationships for use in global diagenetic models. *Deep Sea Res. Part I Oceanogr. Res. Pap.* **44**, 327–344 (1997).
20. T. M. Conway, S. G. John, Quantification of dissolved iron sources to the North Atlantic Ocean. *Nature* **511**, 212–215 (2014).
21. M. Labatut *et al*., Iron sources and dissolved-particulate interactions in the seawater of the western equatorial Pacific, iron isotope perspectives. *Global Biogeochem. Cycles* **28**, 1044–1065 (2014).
22. C. Abadie, F. Lacan, A. Radic, C. Pradoux, F. Poitrasson, Iron isotopes reveal distinct dissolved iron sources and pathways in the intermediate versus deep Southern Ocean. *Proc. Natl. Acad. Sci. U.S.A.* **114**, 858–863 (2017).
23. J. N. Fitzsimmons *et al*., Partitioning of dissolved iron and iron isotopes into soluble and colloidal phases along the GA03 GEOTRACES North Atlantic transect. *Deep Sea Res. Part II Top. Stud. Oceanogr.* **116**, 130–151 (2015).
24. R. Schlitzer *et al*., The GEOTRACES intermediate data product 2017. *Chem. Geol.* **493**, 210–223 (2018).
25. K. Kuma, A. Katsumoto, J. Nishioka, K. Matsunaga, Size-fractionated iron concentrations and Fe(III) hydroxide solubilities in various coastal waters. *Estuar. Coast. Shelf Sci.* **47**, 275–283 (1998).
26. K. Dideriksen, J. A. Baker, S. L. S. Stipp, Fe isotope fractionation between inorganic aqueous Fe(III) and a Fe siderophore complex. *Mineral. Mag.* **72**, 313–316 (2008).
27. K. Kunde *et al*., Iron distribution in the subtropical North Atlantic: The pivotal role of colloidal iron. *Global Biogeochem. Cycles* **33**, 1532–1547 (2019).
28. W. B. Homoky *et al*., Iron and manganese diagenesis in deep sea volcanogenic sediments and the origins of pore water colloids. *Geochim. Cosmochim. Acta* **75**, 5032–5048 (2011).
29. W. D. Gardner, M. J. Richardson, A. V. Mishonov, Global assessment of benthic nepheloid layers and linkage with upper ocean dynamics. *Earth Planet. Sci. Lett.* **482**, 126–134 (2018).
30. J. C. Latimer, G. M. Filippelli, Sedimentary iron records from the Cape Basin. *Deep Sea Res. Part II Top. Stud. Oceanogr.* **54**, 2422–2431 (2007).
31. W. Weijer, M. E. Maltrud, W. B. Homoky, K. L. Polzin, L. R. M. Maas, Eddy-driven sediment transport in the Argentine Basin: Is the height of the Zapiola Rise hydrodynamically controlled? *J. Geophys. Res. Oceans* **120**, 2096–2111 (2015).
32. R. C. Thunell, Carbonate dissolution and abyssal hydrography in the Atlantic Ocean. *Mar. Geol.* **47**, 165–180 (1982).
33. T. J. Shaw, J. M. Gieskes, R. A. Jahnke, Early diagenesis in differing depositional environments: The response of transition metals in pore water. *Geochim. Cosmochim. Acta* **54**, 1233–1246 (1990).
34. B. L. Beard *et al*., Application of Fe isotopes to tracing the geochemical and biological cycling of Fe. *Chem. Geol.* **195**, 87–117 (2003).
35. A. Dutkiewicz, R. D. Müller, S. O'Callaghan, H. Jónasson, Census of seafloor sediments in the world's ocean. *Geology*, **43**, 795–798 (2015).
36. R. N. Glud, Oxygen dynamics of marine sediments. *Mar. Biol. Res.* **4**, 243–289 (2008).
37. P. N. Froelich *et al*., Early oxidation of organic matter in pelagic sediments of the eastern equatorial Atlantic: Suboxic diagenesis. *Geochim. Cosmochim. Acta* **43**, 1075–1090 (1979).
38. S. Henkel, S. Kasten, J. F. Hartmann, A. Silva-Busso, M. Staubwasser, Iron cycling and stable Fe isotope fractionation in Antarctic shelf sediments, King George Island. *Geochim. Cosmochim. Acta* **237**, 320–338 (2018).
39. S. Henkel, S. Kasten, S. W. Poulton, M. Staubwasser, Determination of the stable iron isotopic composition of sequentially leached iron phases in marine sediments. *Chem. Geol.* **421**, 93–102 (2016).
40. L. Wu, B. L. Beard, E. E. Roden, C. M. Johnson, Stable iron isotope fractionation between aqueous Fe(II) and hydrous ferric oxide. *Environ. Sci. Technol.* **45**, 1847–1852 (2011).
41. B. L. Beard *et al*., Iron isotope fractionation between aqueous ferrous iron and goethite. *Earth Planet. Sci. Lett.* **295**, 241–250 (2010).
42. A. J. Birchill *et al*., Seasonal iron depletion in temperate shelf seas. *Geophys. Res. Lett.* **44**, 8987–8996 (2017).
43. M. Gledhill, K. N. Buck, The organic complexation of iron in the marine environment: A review. *Front. Microbiol.* **3**, 69 (2012).
44. P. H. Santschi, Marine colloids, agents of the self-cleansing capacity of aquatic systems: Historical perspective and new discoveries. *Mar. Chem.* **207**, 124–135 (2018).
45. M. L. Wells, E. D. Goldberg, Marine submicron particles. *Mar. Chem.* **40**, 5–18 (1992).
46. R. Raiswell, D. E. Canfield, The iron biogeochemical cycle past and present. *Geochem. Perspect.* **1**, 1–2 (2012).
47. C. van der Zee, D. R. Roberts, D. G. Rancourt, C. P. Slomp, Nanogoethite is the dominant reactive oxyhydroxide phase in lake and marine sediments. *Geology* **31**, 993–996 (2003).
48. A. Gartman, A. J. Findlay, G. W. Luther III, Nanoparticulate pyrite and other nanoparticles are a widespread component of hydrothermal vent black smoker emissions. *Chem. Geol.* **366**, 32–41 (2014).
49. A. D. Anbar, O. Rouxel, Metal stable isotopes in paleoceanography. *Annu. Rev. Earth Planet. Sci.* **35**, 717–746 (2007).
50. E. Lotfi-Kalahroodi *et al*., Iron isotope fractionation in iron-organic matter associations: Experimental evidence using filtration and ultrafiltration. *Geochim. Cosmochim. Acta* **250**, 98–116 (2019).
51. M. T. Jones *et al*., Quantifying the impact of riverine particulate dissolution in seawater on ocean chemistry. *Earth Planet. Sci. Lett.* **395**, 91–100 (2014).
52. C. Jeandel, Overview of the mechanisms that could explain the 'Boundary Exchange' at the land-ocean contact. *Philos. Trans. A Math. Phys. Eng. Sci.* **374**, 20150287 (2016).
53. L. K. ThomasArrigo, J. M. Byrne, A. Kappler, R. Kretzschmar, Impact of organic matter on iron(II)-catalyzed mineral transformations in ferrihydrite-organic matter coprecipitates. *Environ. Sci. Technol.* **52**, 12316–12326 (2018).
54. K. Lalonde, A. Mucci, A. Ouellet, Y. Gélinas, Preservation of organic matter in sediments promoted by iron. *Nature* **483**, 198–200 (2012).
55. K. A. Lettmann *et al*., Estimation of biogeochemical rates from concentration profiles: A novel inverse method. *Estuar. Coast. Shelf Sci.* **100**, 26–37 (2012).
56. K. Laufer, H. Røy, B. B. Jørgensen, A. Kappler, Evidence for the existence of autotrophic nitrate-reducing Fe(II)-oxidizing bacteria in marine coastal sediment. *Appl. Environ. Microbiol.* **82**, 6120–6131 (2016).
57. C. M. Johnson, E. E. Roden, S. A. Welch, B. L. Beard, Experimental constraints on Fe isotope fractionation during magnetite and Fe carbonate formation coupled to dissimilatory hydrous ferric oxide reduction. *Geochim. Cosmochim. Acta* **69**, 963–993 (2005).

58. L. Wu, G. Druschel, A. Findlay, B. L. Beard, C. M. Johnson, Experimental determination of iron isotope fractionations among Fe2+(aq)-FeS(aq)-Mackinawite at low temperatures: Implications for the rock record. *Geochim. Cosmochim. Acta* **89**, 46–61 (2012).
59. S. M. Kraemer, Iron oxide dissolution and solubility in the presence of siderophores. *Aquat. Sci.* **66**, 3–18 (2004).
60. J. G. Wiederhold *et al*., Iron isotope fractionation during proton-promoted, ligand-controlled, and reductive dissolution of Goethite. *Environ. Sci. Technol.* **40**, 3787–3793 (2006).
61. C. B. Kennedy, S. D. Scott, F. G. Ferris, Hydrothermal phase stabilization of 2-line ferrihydrite by bacteria. *Chem. Geol.* **212**, 269–277 (2004).
62. F. Couceiro *et al*., Impact of resuspension of cohesive sediments at the Oyster Grounds (North Sea) on nutrient exchange across the sediment–water interface. *Biogeochemistry* **113**, 37–52 (2013).
63. D. A. Cacchione, W. D. Grant, D. E. Drake, S. M. Glenn, Storm-dominated bottom boundary layer dynamics on the Northern California continental shelf: Measurements and predictions. *J. Geophys. Res.* **92**, 1817–1827 (1987).
64. D. A. Cacchione, L. F. Pratson, A. S. Ogston, The shaping of continental slopes by internal tides. *Science* **296**, 724–727 (2002).
65. T. Stratmann, K. Soetaert, C.-L. Wei, Y.-S. Lin, D. van Oevelen, The SCOC database, a large, open, and global database with sediment community oxygen consumption rates. *Sci. Data* **6**, 242 (2019).
66. L. Bridgestock *et al*., Controls on the barium isotope compositions of marine sediments. *Earth Planet. Sci. Lett.* **481**, 101–110 (2018).
67. R. A. Mortlock, P. N. Froelich, A simple method for the rapid determination of biogenic opal in pelagic marine sediments. *Deep-Sea Res. A Oceanogr. Res. Pap.* **36**, 1415–1426 (1989).
68. T. M. Conway, A. D. Rosenberg, J. F. Adkins, S. G. John, A new method for precise determination of iron, zinc and cadmium stable isotope ratios in seawater by double-spike mass spectrometry. *Anal. Chim. Acta* **793**, 44–52 (2013).
69. T. M. Conway, S. G. John, F. Lacan, Intercomparison of dissolved iron isotope profiles from reoccupation of three GEOTRACES stations in the Atlantic Ocean. *Mar. Chem.* **183**, 50–61 (2016).
70. E. Precht, M. Huettel, Advective pore-water exchange driven by surface gravity waves and its ecological implications. *Limnol. Oceanogr.* **48**, 1674–1684 (2003).
71. H. Planquette, R. R. Sanders, P. J. Statham, P. J. Morris, G. R. Fones, Fluxes of particulate iron from the upper ocean around the Crozet Islands: A naturally iron-fertilized environment in the Southern Ocean. *Global Biogeochem. Cycles* **25**, GB2011 (2011).